J. Membrane Biol. 214, 59–73 (2006)
DOI: 10.1007/s00232-006-0078-2

The Journal of
Membrane
Biology

A Mathematical Model of the Diluting Power of the Cortical Thick Ascending Limb of the Loop of Henle

João C. Dias[1], Frederico C. Ferreira[1,2], Hugo G. Ferreira[1], Teresa F. Moura[1]
[1]REQUIMTE, Departamento de Química, Faculdade de Ciências e Tecnologia, Universidade Nova de Lisboa, 2829-516, Caparica, Portugal
[2]Imperial College London, Department of Chemical Engineering and Chemical Technology, South Kensington Campus SW7 2AZ., U.K.

Received: 25 September 2006/Revised: 7 November 2006

Abstract. A mathematical model is presented that describes the ionic transport across the cortical thick ascending limb (cTAL) of the Henle's loop, taking into account its tubular geometry. A comprehensive description of the cTAL is given for the first time in terms of potential, ion concentrations and ion fluxes along the tubule. For given ion concentrations at the entrance of the tubule, the model simulates steady-state profiles and allows the fitting of existing experimentally measured values at its exit. Moreover, the model expands the potentialities of experiments *in situ* and enables testing the effect of different perturbations induced by drugs or mutation-altering transport activity. One of the main insights given by this model is the increase of the lumenal electrical potential from the entrance to the exit of the tubule with a profile determined by the transepithelial electrical potential difference and by the chemical gradients along the lumen, both reflecting transepithelial salt transport. Furthermore, model and experimental results are consistent, showing that when the TAL is perfused at high rates with a diluted NaCl solution in relation to the bath, the transepithelial electrical potential difference increases from 6.7 to 23.0 mV and the potential difference across the basolateral barrier changes very little. The model predicts that the same static head is obtained independently of the NaCl concentration at the entrance of the tubule. A final important insight concerns the lowest reported NaCl concentrations (20–30 mM) at the exit of the tubule, which is controlled by a very tight epithelium, where the back-leak is substantially reduced.

Key words: Nephron — Tubular epithelium — Salt transport — Mathematical model — Numerical simulation

Correspondence to: Teresa F. Moura; email: tfm@dq.fct.unl.pt

Introduction

The production of concentrated urine in the mammalian kidney results from the combination of the transport activity of the nephrons with their three-dimensional arrangement (Wirz, Hargitay & Kuhn, 1951). Therefore, the study of kidney function has been focused on the characterization of its anatomofunctional components (transport systems, cells, tubules, vessels, etc.) and on the construction of mathematical models encoding these data together with the geometrical factors. A considerable number of these models have been published (Stephenson, 1992; Weinstein, 1994; Wexler, Kalaba & Marsh, 1991) covering from segments of the nephrons (Weinstein, 2003) to multitube units including the vascular component (Stephenson, 1992).

Experimental studies to obtain key morphological and kinetic parameters and to test mathematical models would ideally be performed for the same animal and under the same physiological situations. This is not always possible. Some segments of the nephrons can be approached *in situ* by micropuncture techniques (proximal and distal tubules, collecting ducts, etc.), while others remain inaccessible to this approach. Such is the case of the cortical thick ascending limb (cTAL) of the loop of Henle. Published *in vitro* perfusion experimental studies, however, cover all the nephron segments. In particular, Greger (1985) studied in great detail the rabbit cTAL using high perfusion rates, under which the system can be treated as a flat sheet bathed by two semi-infinite compartments. Fernandes & Ferreira (1991) modeled their results with reasonable fidelity (FF model).

To simulate the behavior of the cTAL under *in situ* conditions, we present an expansion of the FF model by encoding the geometric properties of a tube. In the present work, we built a water-impermeable tubular extension of the flat sheet FF model in which,

as the fluid flows in the lumen, salt reabsorption occurs through the walls and a hypotonic fluid is produced at the exit of the tubule (Burg, 1982; Greger, 1985; Jamison & Gehrig, 1992). In this system, ion transport is now dependent on the rate of volume flow. The present model differs from that of Reeves, Molony & Andreoli (1988) because it considers the tubular geometry and the transporting barrier is described as a proper epithelium comprising the cell compartment and including diffusional and mediate ion fluxes. Such tubular expansion of the flat sheet FF model entails the ability to predict other aspects of the system behavior such as changes in cell volume, paracellular and transcellular ion fluxes and the behavior of the apical and basolateral membranes. The model was developed using the Berkeley Madonna software (http://www.berkeleymadonna.com/).

Transient and steady-state simulations are presented in order to understand and to evaluate cTAL performance and the physiological mechanisms. In the absence of *in situ* experimental studies for this nephron segment, the model was tested against experimental *in vitro* data. Therefore, model input conditions were selected according to the conditions used in previously published experimental studies (Greger, 1981, 1985; Burg & Green, 1973; Reeves et al., 1988; Katz, Doucet & Morel, 1979; Rocha & Kokko, 1973; Greger & Schlatter, 1983; Wirz et al., 1951; Oberleithner et al., 1982; Greger et al., 1983, 1984) and the calculated output variables are compared with their experimental measured values (Burg & Green, 1973; Rocha & Kokko, 1973; Imai, 1977).

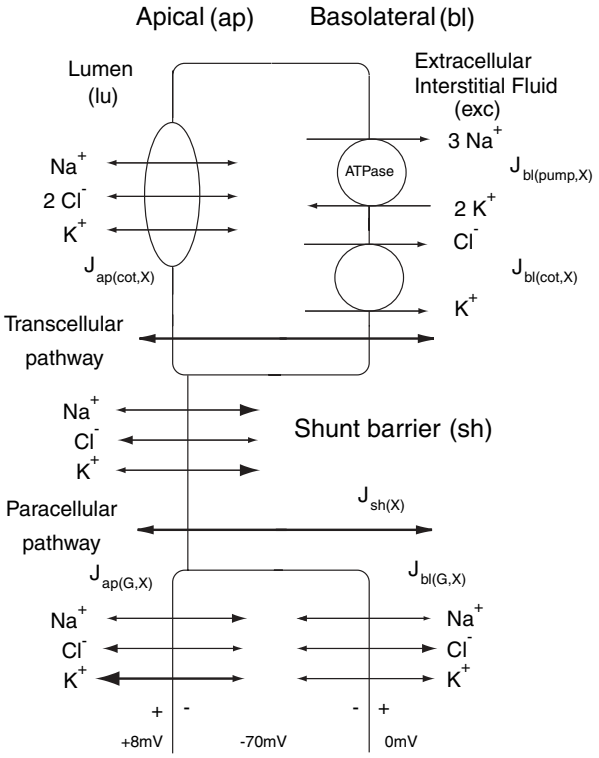

Fig. 1. Epithelial cell model for cTAL, according to the flat sheet FF model (Fernandes & Ferreira, 1991), with two parallel pathways, transcellular and paracellular. The transcellular pathway comprises two barriers, the apical and the basolateral, in series with the cytoplasm. In the apical membrane, there are Na^+-$2Cl^-$-K^+ cotransport ($J_{ap(cot,X)}$) and channels for Na^+, K^+ and Cl^- ($J_{ap(G,X)}$). In the basolateral membrane, there are Na^+-K^+-ATPase ($J_{bl(pump,X)}$), K^+-Cl^- cotransport ($J_{bl(cot,X)}$) and channels for the three ions ($J_{bl(G,X)}$). In the paracellular pathway (shunt), there are conductances for the three ions ($J_{sh(G,X)}$). The weights of the *arrows* in the Goldman fluxes indicate the direction of the net fluxes in the reference state.

Methods

Numerical Model

Our mathematical model is a tubular extension of the flat sheet FF model where transepithelial ion fluxes (diffusional and mediated) are taken into account, as shown in Figure 1. As described (Fernandes & Ferreira, 1991) under open circuit conditions, net transport of NaCl from the lumen to the extracellular interstitial compartments is driven by the Na^+/K^+-ATPase. No net transport of K^+ across the epithelium is detected as the K^+ recirculates in both cellular barriers. In the apical barrier it enters through Na^+-$2Cl^-$-K^+ cotransport and leaves through a diffusional pathway (channels), while in the basolateral barrier it enters via Na^+/K^+-ATPase and leaves through K^+-Cl^- cotransport and K^+ channels. The lumen-positive potential difference drives the positive ions toward the extracellular interstitium, while the Cl^- ions move in the opposite direction through the diffusional junction pathway. Under steady-state and open circuit conditions, two Cl^- ions per one Na^+ cross the cells, thus creating a positive circulating current as one Cl^- ion moves through the junctions back to the lumen. The flat sheet FF model considers the flat epithelial sheet separating two semi-infinite compartments, so the ion concentrations in both extracellular mediums remain constant. Interestingly, as we extend this model to a tubular geometry, concentrations along the tubule lumen decrease due to NaCl reabsorption; this changes the driving force for the transepithelial NaCl fluxes and eventually leads to inversion of the Na^+ flux across the junction pathway. Consequently, inclusion of the tubular geometrical characteristic in the FF model is essential for the description of cTAL function and evaluation of its physiological performance.

For the tubular model, all the nomenclature used is summarized in Appendix 1.

Geometry of the cTAL and Composition of Fluids

For the rabbit kidney, the tubule is a cylinder with an internal radius (r) in the range 6-12 μm (Katz et al., 1979; Greger, 1981; Reeves et al., 1988), a cell wall thickness (τ) of 1-2 μm (Greger, 1985) and a tubule length (L) usually varying 1.05-1.65 mm (Burg & Green, 1973) but L values as high as 3.4 mm are also reported (Reeves et al., 1988). The experimental data available for the rabbit and mouse tubules (Burg & Green, 1973; Reeves et al., 1988; Rocha & Kokko, 1973) perfused at flow rates (f) varying 0.4-2.8 nl · min^{-1} showed a decrease in osmolarity along the tubule lumen. To achieve constancy of perfusate composition, other authors (Greger & Schlatter, 1983) used much higher f values (10-20 nl · min^{-1}).

We considered the L value fixed at 1 mm and f values around 1 nl · min^{-1}, corresponding to a linear flow rate of 3.18 mm · min^{-1},

Table 1. Model parameters and reference state input/output values

	P_{x_Ref} (Cm-s^{-1}) $\times 10^7$			K (mM)			[X] (mM)	
	ap	*bl*	*sh*	*ap_cot*	*Pump*	*bl_cot*	*Exc*	Cell
Na^+	0.36*	0.41*	246*	2.5	2.6		145	15
K^+	1,843*	100*	295*	1.5	0.56		5	145
Cl^-	5.0*	440*	98*	55				29
J_{mx} (nmol·cm^{-2}·s^{-1})				3.1*	1.1*	2.8 x 10^8*		
V (mV)	78	−70	8					
I_{tot} (μA·cm^{-2})			−150					
A								111*
z_A								−1.2*
r = 10 μm	τ = 1.5 μm	f = 1 nl·min^{-1}	L = 1 mm					

Initial values for the intracellular (*Cell*) and extracellular (*Exc*) ion concentrations and electrical potential differences and the values of some of the parameters taken directly from the literature. *Values of the remaining parameters of the model that were calculated in the reference state according to the flat sheet FF model (Fernandes & Ferreira, 1991).

when analyzing the dependence of the model on several parameters. However, f values have been varied from 0.01 to 2 nl · min^{-1} when studying the effect of f/L. A τ value of 1.5 μm was assumed for all model calculations.

Three compartments were taken into account: the cell (*c*), the lumen (*lu*) and the extracellular interstitial fluid (*exc*). The model applies to the cortical portion of the TAL, where the osmolarity of the extracellular interstitial fluid (osm_{exc}) is considered constant (Wirz et al., 1951) over its whole length and where the fluid at the entrance of the tubule lumen is isotonic with the extracellular interstitial fluid. According to Greger (1985), Na^+, K^+ and Cl^- are the only electrophysiologically relevant ions in these fluids; and the respective extracellular concentrations used were 145, 5, 150 mM, with a total osmolarity of 300 mOsm.

It is assumed that cells only contain as diffusible species Na^+, K^+ and Cl^- at the respective initial concentrations of 15 mM (Oberleithner et al., 1982), 145 mM (Greger et al., 1984) and 29 mM (Greger et al., 1983). The quantity of the nondiffusible anions (Q_A) and their average valence (z_A) are adjusted initially in the model, considering that the cells are in osmotic equilibrium with the extracellular interstitial fluid and that electroneutrality applies in the cell compartment.

Model Parameters and Input Variables

The flat sheet FF model has the following parameter types, which are also used in the tubular model (Table 1):

- $P_{M(X)}$ - The nine permeabilities of the three barriers (M) of the epithelium for the three diffusible ions (X, with valence z_X). The barriers considered are the apical (*ap*) and basolateral (*bl*) membranes and the junctions also called the shunt pathway (*sh*). The diffusible ions are chloride (Cl^-), potassium (K^+) and sodium (Na^+).
- $J_{M(Tr,mx)}$ - The three maximum fluxes (*mx*) of the mediated transporters (*Tr*) located in the barrier (M): the Na^+-2Cl^--K^+ cotransport (*cot*) in the apical barrier, the K^+-Cl^- cotransport (*cot*) and the Na^+-K^+-ATPase pump (*pump*) in the basolateral barrier.
- $K_{M(Tr,X)}$ - The three affinity constants for the cotransport in the apical membrane and two affinity constants for the pump in the basolateral membrane.

Additional parameters were included for the tubular model of cTAL: Q_A, z_A, τ, r, f and L.

Some values of the model parameters were taken directly from the literature, while others were calculated using the strategy adapted from the flat sheet FF model (Fernandes & Ferreira, 1991) for the reference state (summarized in Appendix 2, eq. 1a-32a). The calculations take into account: (1) reliable stabilized interrelations between ion fluxes (eq. 1a-6a) and $P_{sh(X)}$ value ratios (eq. 7a-8a); (2) charge, tonicity and mass conservation principles (eq. 9a-16a); (3) diffusional fluxes follow the Goldman Hodgkin and Katz equation (eq. 17a-25a); (4) mediated fluxes follow particular kinetics (eq. 26a-32a). The flat sheet FF model calculates the reference state values for the nine $P_{M(X)}$, the three $J_{M(Tr,mx)}$, Q_A and z_A. These values (Table 1) are used as parameters in the tubular model.

The nine diffusible ion concentrations ($[X]_{CP\_Ref}$) in the three compartments (*CP*) and the volume of the cell compartment ($volu_{c\_Ref}$) are used as input variables in the flat sheet FF model (reference state) and remain constant during the computations of the parameters. However, for the tubular model, only the three extracellular interstitial ion concentrations ($[X]_{exc}$) used as input variables remain constant and at the same value for all the n-segments during the whole simulation. Additionally, the input values for the three ion concentrations at the entrance of the tube lumen remain constant, $[X]_{lu(i=0)}$.

Tubular Model of cTAL

Our numerical strategy is similar to that used by Chang & Fujita (1999) for the distal tubule. An epithelial tubule is divided into n cylindrical segments, each with characteristics corresponding to the FF model and dimensions r, τ and segment height Δx (= L/n). This strategy simplifies the calculus as the differential equations used in the model for each i-segment are only a function of time. The dependence on tubule position will be determined by the values of the different variables computed for the different i-segments.

The cylinder epithelial walls are water-impermeable and reabsorb NaCl from the flowing lumenal fluid. The composition of the extracellular interstitial fluid is assumed constant, corresponding to a semi-infinite compartment. The tubular model was built in two steps. In the first step, the tubule lumen is filled with a fluid with the same composition as the extracellular interstitial fluid (*exc*, Table 1). In the second step, this fluid is fed into the entrance of the lumen tube (with constant ion concentrations, $[X]_{lu,i=0}$) at a constant flow rate (f) and the transepithelial ion fluxes across the n-segments are then computed until a steady state is reached (control state). This steady state corresponds to an established profile of decreasing concentrations along the tube lumen, assuming homogeneous solution in each segment for the lumen and cell compartments; radial lumen concentration gradients were not taken into account. The variables are computed for the entrance and exit of each i-segment, thus giving a total of n + 1 values. The

composition of the fluid collected at the exit of the tubule is taken as the one in the last segment.

The variables computed (dependent on time and position of the tubule) are as follows:

- The nine diffusional fluxes ($J_{M(G,X,i)}$) through apical and basolateral membranes and junction pathway and the seven mediated fluxes ($J_{M(Tr,X,i)}$) for the diffusible ions. Fluxes are considered positive in the direction lumen to cell to extracellular interstitial fluid (eq. 1-16).
- The concentrations $[X]_{CP(i)}$ of the three diffusible ions in each of the compartments (*CP*), intracellular (*c*) and lumen (*lu*); the intracellular concentration of nondiffusible species $[A]_{c(i)}$; and the osmolarity of the lumen ($osm_{lu(i)}$) (eq. 17-24).
- The volume of the intracellular compartment ($volu_{c(i)}$) (eq. 25).
- The quantities $Q_{CP(X,i)}$ of the three diffusible ions in each of the compartments (*CP*), intracellular (*c*) and lumen (*lu*) (eq. 26-31).
- The three dimensionless potential differences across the three barriers ($E_{ap(i)}$, $E_{bl(i)}$, $E_{OC(i)}$) (eq. 32-34).

The tubular model considers the parameter values and the initial values for all variables equal to their reference state values (Table 1). Furthermore, the kinetic equations describing the ion fluxes in each *i*-segment (eq. 1-16) and the three saturation ratios are identical to the equations used in the reference state, taking into account the appropriate replacement for the ion concentrations and for the electrical potential differences for that specific *i*-segment. The nine diffusional fluxes $J_{M(G,X,i)}$ were calculated assuming the Goldman Hodgkin and Katz equation:

$$J_{M(G,X,i)} = P_{M(X)} \cdot \left([X]_{CP1(i)} \cdot e^{z_X \cdot E_{M(i)}} - [X]_{CP2(i)} \right) \cdot Z_X \cdot E_{M(i)} \Big/ \left(e^{z_X \cdot E_{M(i)}} - 1 \right) \qquad \text{eq.1} - 9$$

The two Na^+-K^+ pump fluxes were calculated as follows:

$$J_{bl(pump,Na,i)} = J_{bl(pump,mx)} \cdot Sat_{bl(pump,i)} \qquad \text{eq.10} - 11$$

$$J_{bl(pump,K,i)} = -(2/3) \cdot J_{bl(pump,Na,i)}$$

with

$$Sat_{bl(pump,i)} = \left[1 \Big/ \left[1 + \frac{K_{bl(pumpNa)}}{[Na]_{c(i)}} \right] \right]^3 \cdot \left[1 \Big/ \left[1 + \frac{K_{bl(pumpK)}}{[K]_{exc(i)}} \right] \right]^2$$

The three Na^+-K^+-$2Cl^-$ cotransport fluxes were calculated as follows:

$$J_{ap(\mathrm{cot},Na,i)} = J_{ap(\mathrm{cot},mx)} \cdot Sat_{ap(\mathrm{cot},i)} \qquad \text{eq.12} - 14$$

$$J_{ap(\mathrm{cot},K,i)} = J_{ap(\mathrm{cot},Na,i)}$$

$$J_{ap(\mathrm{cot},Cl,i)} = 2 \cdot J_{ap(\mathrm{cot},Na,i)}$$

with

$$Sat_{ap(\mathrm{cot},i)} = \left[1 \Big/ \left[1 + \frac{K_{ap(\mathrm{cot},Na)}}{[Na]_{lu(i)}} \right] \right] \cdot \left[1 \Big/ \left[1 + \frac{K_{ap(\mathrm{cot},K)}}{[K]_{lu(i)}} \right] \right] \cdot \left[1 \Big/ \left[1 + \frac{K_{ap(\mathrm{cot},Cl)}}{[Cl]_{lu(i)}} \right] \right]^2 - \left[1 \Big/ \left[1 + \frac{K_{ap(\mathrm{cot},Na)}}{[Na]_{c(i)}} \right] \right] \cdot \left[1 \Big/ \left[1 + \frac{K_{ap(\mathrm{cot},K)}}{[K]_{c(i)}} \right] \right] \cdot \left[1 \Big/ \left[1 + \frac{K_{ap(\mathrm{cot},Cl)}}{[Cl]_{c(i)}} \right] \right]^2$$

Finally, the two K^+-Cl^- cotransport fluxes were calculated as follows:

$$J_{bl(\mathrm{cot},K,i)} = J_{bl(\mathrm{cot},mx)} \cdot Sat_{bl(\mathrm{cot},i)} \qquad \text{eq.15} - 16$$

$$J_{bl(\mathrm{cot},Cl,i)} = J_{bl(\mathrm{cot},K,i)}$$

with

$$Sat_{bl(\mathrm{cot},i)} = [Cl]_{c(i)}[K]_{c(i)} - [Cl]_{exc(i)}[K]_{exc(i)}$$

The concentrations of the three diffusible ions in the lumen (eq. 17−19) and cell compartments $[X]_{CP(i)}$ (eq. 20−22) and of the nondiffusible species concentration $[A]_{c(i)}$ (eq. 23) are calculated from the ratio of their respective quantities ($Q_{CP(X,i)}$, Q_A) and compartment volumes ($volu_{CP(i)}$):

$$[X]_{lu(X,i)} = Q_{lu(X,i)} / volu_{lu(i)} \qquad \text{eq.17} - 23$$

$$[X]_{c(X,i)} = Q_{c(X,i)} / volu_{c(i)}$$

$$[A]_{c(i)} = Q_A / volu_{c(i)}$$

The lumen osmolarity ($osm_{lu(i)}$) is calculated as the sum of the ion concentrations in the lumen for each segment:

$$osm_{lu(i)} = [Na]_{lu(i)} + [K]_{lu(i)} + [Cl]_{lu(i)} \qquad \text{eq.24}$$

Furthermore, for each *i*-segment, the model equation system is comprised of a tonicity balance equation (eq. 25) and eight differential equations (eq. 26-33) to calculate nine variables: the $volu_{c(i)}$, the six $Q_{CP(i)}$ and the two $V_{M(i)}$.

The $volu_{c(i)}$ is calculated by the tonicity balance equation that describes the osmotic equilibrium between intracellular and extracellular interstitial fluid, considering osm_{exc} = 300 mOsm and the initial value of $volu_{c\_\mathrm{Ref}}$ defined in Appendix 1. Q_A is an input variable calculated in the reference state that remains constant at the same value for all the *n*-segments throughout the calculations.

$$volu_{c(i)} = \left(Q_{c(Na,i)} + Q_{c(K,i)} + Q_{c(Cl,i)} + Q_A \right) / osm_{exc} \qquad \text{eq.25}$$

Three of the differential equations (eq. 26−28) are mass balances for the intracellular ion quantities for each *i*-segment:

$$d/dt\left(Q_{c(Na,i)}\right) = J_{ap(G,Na,i)} + J_{ap(\mathrm{cot},i)} - 3J_{bl(pump,i)} - J_{bl(G,Na,i)} \qquad \text{eq.26} - 28$$

$$d/dt\left(Q_{c(K,i)}\right) = J_{ap(G,K,i)} + J_{ap(\mathrm{cot},i)} + 2J_{bl(pump,i)} - J_{bl(G,K,i)} - J_{bl(\mathrm{cot},i)}$$

$$d/dt\left(Q_c(cl,i)\right) = J_{ap(G,Cl,i)} + 2J_{ap(\mathrm{cot},i)} - J_{bl(G,Cl,i)} - J_{bl(\mathrm{cot},i)}$$

For each *i*-segment, the lumen volume ($volu_{lu(i)}$) and the wall area (Ar) are constant and equal to $\tilde{\pi} \cdot r^2 \cdot \Delta x$ and $2 \cdot \pi r \cdot \Delta x$, respectively. Lumen ion quantities in the different segments are calculated from the differences between the quantities that enter and exit each segment. The entrance is the quantity that leaves the previous lu-

men segment $f \cdot [X]_{lu(i-1)}$, while the exit has two components, the transfer of the fluid to the next segment $f \cdot [X]_{lu(i)}$ and the reabsorption of the epithelial cells $Ab_{(X,i)}$, where X is the diffusible ion species (Na^+, K^+ or Cl^-). Therefore, three of the differential equations (eq. 29-31) are mass balances for the lumen ion quantities for each i-segment:

$$d/dt\left(Q_{lu(X,i)}\right) = f \cdot \left([X]_{lu(i-1)} - [X]_{lu(i)}\right) - Ab_{(X,i)} \qquad \text{eq.29-31}$$

with the absorption rate ($Ab_{(X,i)}$) of X through the epithelial wall of each i-segment defined as follows:

$$Ab_{(X,i)} = Ar \cdot \left(J_{ap(\cot,X,i)} + J_{ap(G,X,i)} + J_{sh(G,X,i)}\right)$$

For example, for the first two segments, eq. 29–31 would be written as follows:

$$d/dt\left(Q_{lu(X,1)}\right) = f \cdot \left([X]_{lu(0)} - [X]_{lu(1)}\right) - Ab_{(X,1)}$$
$$d/dt\left(Q_{lu(X,2)}\right) = f \cdot \left([X]_{lu(1)} - [X]_{lu(2)}\right) - Ab_{(X,2)}$$

Thus, generally:

$$d/dt\left(Q_{lu(X,i)}\right) = f \cdot \left([X]_{lu(i-1)} - [X]_{lu(i)}\right) - Ab_{(X,i)}$$

Notice that for the entrance of the first segment, $[X]_{lu,i=0}$ takes the value given to the model as an input variable, whereas for the subsequent segments $[X]_{lu,i\geq 1}$ values are calculated by the model (eq. 17-19).

The potential difference across a barrier is evaluated taking into account the relation $V = Q_{ch}/C_M$, where Q_{ch} is the total electrical charge and C_M is the membrane capacitance. If ions flow across the barrier, the total electrical charge may be altered and V will change accordingly:

$$\frac{dV}{dt} = \frac{1}{C_M}\frac{dQ_{ch}}{dt}$$

with

$$\frac{dQ_{ch}}{dt} = I_{total} = \sum_X (F \cdot z_X \cdot J_X)$$

therefore

$$\frac{dV}{dt} = \frac{F}{C_M}\sum_X z_x \cdot J_X$$

The electrical potential differences $V_{Oc(i)}$ and $V_{M(i)}$ are converted into the dimensionless variables $E_{OC(i)}$ and $E_{M(i)}$, respectively, as defined in Appendix 1. So for each i-segment, the potential differences $E_{ap(i)}$ and $E_{bl(i)}$ will depend upon the net charge fluxes. As both cotransports are electroneutral, only the diffusional and pump fluxes are considered:

$$d/dt\left(E_{ap(i)}\right) = -factor \cdot \left(J_{ap(G,Na,i)} + J_{ap(G,K,i)} + J_{bl}(Pump,i) - J_{ap(G,Cl,i)} + J_{sh(G,Na,i)} + J_{sh(G,K,i)} - J_{sh(G,Cl,i)}\right) \qquad \text{eq.32-33}$$
$$d/dt\left(E_{bl(i)}\right) = -factor \cdot \left(J_{bl(G,Na,i)} + J_{bl(G,K,i)} + J_{bl(Pump,i)} - J_{bl(G,Cl,i)} + J_{sh(G,Na,i)} + J_{sh(G,K,i)} - J_{sh(G,Cl,i)}\right)$$

The total transepithelial potential difference $E_{OC(i)}$ is the sum of $E_{ap(i)}$ with $E_{bl(i)}$:

$$E_{oc(i)} = E_{ap(i)} + E_{bl(i)} \qquad \text{eq.34}$$

It has been conventional to find approximations (albeit very good ones) to the membrane potential using electroneutrality. However, the use of such approximations can be difficult as it requires the finding of numerical roots of complex systems of nonlinear algebraic equations. Nowadays numerical solutions of differential equations are easier to obtain, so it is more convenient to use this more exact and direct formulation (eq. 32–33). For any plausible capacitance, the time constant is extremely small and, except for an initial very short transient, all the results are totally independent of the value of the capacitance.

The time-dependent differential equations were calculated by the Rosenbrock Stiff method, a variable step-size method (Macey, Oster & Zahnley, 2003), with a tolerance value 10^{-3}, a step-size higher than 0.01 s and an allowed variance for the output steady-state values of 0.007%. Steady state was assumed when calculated output values did not differ with model running time more than 0.001%. This was observed for model running time higher than 35 s. Control steady-state calculations were carried out for a total number of segments, $n = 150$. We verify that further increases in the number of segments do not alter the output values by more than 1.2%. We also estimated that the output values from simulations with 10 and 100 segments did not differ by more than 3%, which is acceptable compared with the associated experimental error. Therefore, in model calculations performed for fitting experimental data, a number of 10 was selected to minimize the time of calculus.

Model Outputs

Among the variables that can be computed (dependent on time and position of the tubule) are the concentration of nondiffusible species, $[A]_{c(i)}$ (eq. 23); the concentrations of the three diffusible ions, $[X]_{CP(i)}$, in the intracellular (eq. 20–22) and lumen (eq. 17–19) compartments; the volume of the intracellular compartment, $volu_{C(i)}$ (eq. 25); the dimensionless potential differences across the cellular barriers, $E_{M(i)}$ (eq. 32–33); all diffusional and mediated fluxes, J (channels, cotransporters, pump and shunt, eq. 1–16); and the osmolarity of the lumen (eq. 24).

In addition, the behavior of another set of variables is analyzed. For each diffusible ion, its total flux across the three barriers is computed as well as its equilibrium potential and the respective ion conductance of the specific barrier.

The total flux ($J_{M(tot,X,i)}$) and equilibrium potential ($Eq_{M(X,i)}$) of X ion across the M barrier are calculated as follows:

$$J_{M(tot,X,i)} = \sum_{Tr} J_{M(Tr,X,i)} + J_{M(G,X,i)} \qquad \text{eq.35-36}$$
$$Eq_{M(X,i)} = 1000 \cdot \ln\left([X]_{CP1}/[X]_{CP2}\right) \cdot RT/(z_x \cdot F)$$

The conductances ($G_{M(X,i)}$, $S \cdot cm^{-2}$) for all three diffusible ions across all barriers are calculated as follows:

$$G_{M(X,z,i)} = \left(P_{M(X,i)} \cdot z_X \cdot F^2\right)/(R \cdot T) \cdot \left(e^{z_x \cdot E_M} - \left(1 + e^{z_x \cdot E_M}\right) \cdot [X]_{CP1} e^{z_x \cdot E_M} - \left((1 - z_x \cdot E_M)e^{zx \cdot EM} - 1\right) \cdot [X]_{CP2}\right)/\left(e^{z_x \cdot E_M} - 1\right)^2 \qquad \text{eq.37}$$

At this stage, an analysis of the functional properties of the system can be performed by looking at the properties of the lumenal fluid along and at the end of the tubule under several geometries, volume flow rates and compositions of the lumenal fluid at the entrance of the tubule. Once the control state was obtained, the model was used

to fit experimental data and to introduce perturbations, such as the effect of transport inhibitors (furosemide, ouabain, etc.).

Results and Discussion

Control state: Behavior of the System at Steady State

Values for some of the parameters in the model were taken directly from the literature (Fernandes & Ferreira, 1991), while the remaining values were computed assuming a steady state (reference state, Table 1). The time and space (position) dependence in the tubular model of the potential differences, cell volume, intracellular and lumen ionic concentrations, ion fluxes of the different transporters on the apical and basolateral membranes as well as shunt pathway were then computed.

The time needed for each variable to reach a steady profile along the tubular segments was different; thus, the total simulation time was chosen to be five times larger than the duration of 90% of the slowest transient. Typical curves for the time dependence of the osmolarity (osm_{lu}) profile are presented in Figure 2a. It can be observed that the steady state is reached within the first 35 s. The remaining panels of Figure 2 report steady-state profiles.

Figure 2b shows that the lumen ion concentrations ($[X]_{lu(i)}$) at the end of the tubule fall to about half their initial values. In particular, Na^+ and Cl^- concentrations decrease to 55%, giving rise to a hypotonic fluid at the exit of the tubule, where the final osmolarity is around 171 mOsm. The total transepithelial ion fluxes ($J_{Tot(X,i)}$) responsible for the formation of the hypotonic fluid along the tubule are represented in Figure 2c. The curve for the total chloride reabsorption is almost identical to that of the total Na^+ reabsorption, a fact that indicates that this epithelium is a sodium chloride transporter, as proposed by Greger & Schlatter (1983). As the fluid in the lumen travels along the tubule, it becomes more and more hypotonic, so the shunt becomes a secreting pathway. As expected, the contribution of this pathway to the fluxes of both ions ($J_{sh(X,i)}$) is different as the transepithelial potential difference (V_{OC}) is lumen-positive. For Cl^-, it is a secreting pathway from the entrance to the exit of the tubule as both concentration and electrical potential gradients are in the same direction (Greger & Schlatter, 1983) (Fig. 2c). For Na^+, however, the contribution of the diffusional driving force due to the Na^+ concentration gradient (toward the lumen) eventually exceeds the electrical driving force (toward the extracellular compartment), thus giving rise to Na^+ secretion toward the end of tubule. Due to the low K^+ concentration in the lumen and extracellular interstitial fluid, the K^+ fluxes across the shunt pathway can be neglected (*not shown*). Figure 2d shows the ion conductances of the shunt pathway ($G_{(sh(X,Tot))}$) along the tubule. Na^+ is the major contributor to the total shunt conductance, followed by Cl^-.

In the model (Fig. 1), the major chloride reabsorption in the apical membrane is due to operation of the Na^+-$2Cl^-$-K^+ cotransport ($J_{ap(cot,Cl)}$), while in the basolateral membrane the chloride movements are due to both K^+-Cl^- cotransport ($J_{bl(cot,Cl)}$) and a Goldman flux ($J_{bl(G,Cl)}$) via chloride channels. Additionally, the results of Figure 2e were obtained taking into account the description of Greger & Schlatter (1983) that the cotransport is responsible for 30% of the total chloride flux in this membrane. As for Na^+, it enters the cell via the cotransport in the apical membrane ($J_{ap(cot,Na)}$) and exits through the pump on the basolateral side ($J_{bl(pump,Na)}$) at a similar rate as the Goldman fluxes ($J_{M(G,Na)}$) across both cellular barriers are so low that they can be ignored (*not shown*). The total pump flux for Na^+ over the whole epithelial cell wall calculated by our model gives a value of 2.9 pmol·cm^{-1}·s^{-1}, which is very similar to the experimental value (2.7 pmol·cm^{-1}·s^{-1}) reported by Katz et al. (1979).

The total transepithelial K^+ flux is much smaller than those of Na^+ and Cl^-, although its flux across the apical barrier ($J_{ap(cot,K)}$) via the cotransporter is very large. This is easily explained by the high K^+ permeability ($P_{ap(K)}$) of the apical membrane that enables the almost total recycling of potassium back to the lumen ($J_{ap(G,K)}$), whereas in the basolateral membrane the pump flux ($J_{bl(pump,K)}$) is canceled out by the sum of the cotransport ($J_{bl(cot,K)}$) and Goldman fluxes ($J_{bl(cot,K)}$) so that the net transfer of potassium across the epithelium is very small (Fig. 2f). These results are in agreement with those reported by Greger & Schlatter (1983).

The intracellular compartment is negative relative to both extracellular compartments. The apical barrier is more polarized than the basolateral barrier with lumen positive in relation to the extracellular interstitial fluid. The K^+ equilibrium potential ($Eq_{ap(K)}$) is the major contributor to the apical potential difference, while for the basolateral electrical potential difference the major contributions are from the K^+ and Cl^- equilibrium potentials ($Eq_{ap(K)}$ and $Eq_{ap(cl)}$) (Table 2).

Although the ion concentrations of the lumenal fluid ($[X]_{lu}$) decrease to almost half of their initial values at the exit of the tubule, the intracellular ion concentrations ($[X]_c$) for Na^+, K^+ and Cl^- only change to 63%, 104% and 76% of their initial values, respectively, and the cell volume ($volu_{c(i)}$) only decreases to 95%.

The potential profiles calculated for V_{OC}, V_{ap} and V_{bl} are almost linear. The maximum deviation from linearity was 15%. As a result of these potential profiles, our model predicts an electrical potential

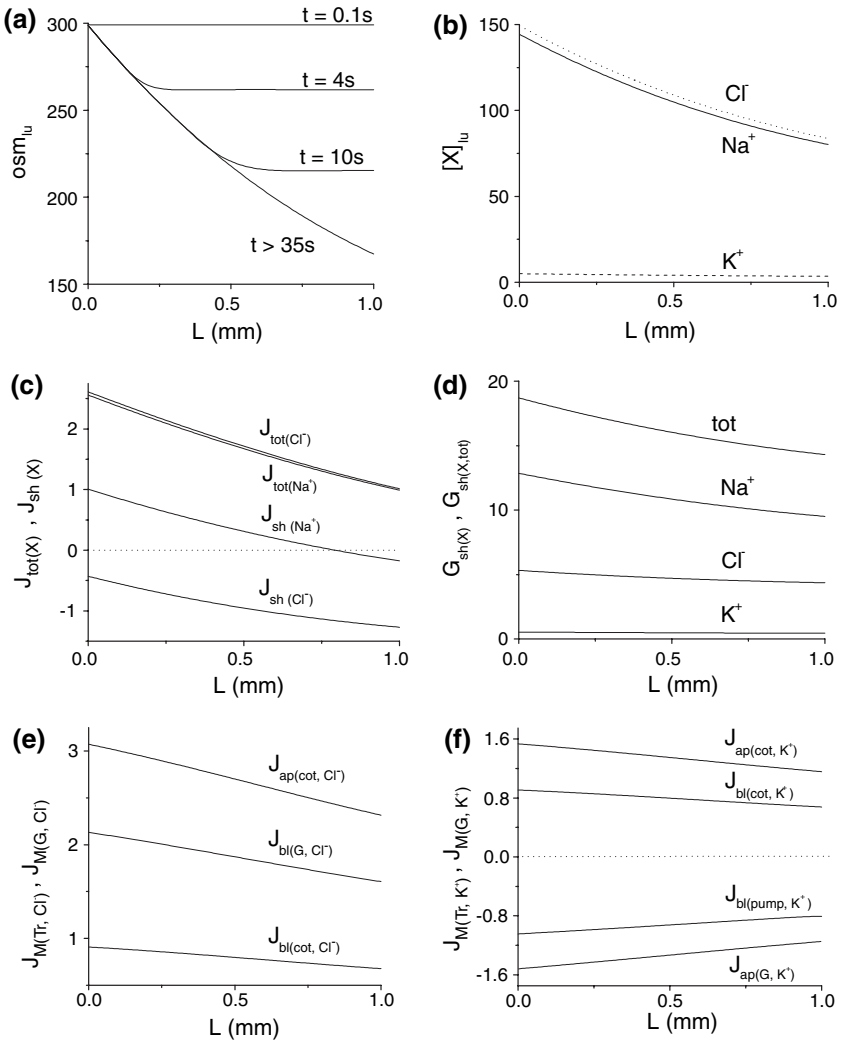

Fig. 2. Profiles for different variables as a function of tubule length (mm). (*a*) Curves showing the evolution of lumen osmolarity (mOsm). Different simulation times (s) (0.1, 4, 10 and >35) were used. After 35 s of simulation, all curves overlap as steady state is reached within this period. (*b*) Lumen ion concentrations (mM). (*c*) Total transepithelial and shunt fluxes for Na^+ and Cl^- (nmol · cm^{-2} · s^{-1}). (*d*) Shunt conductances: total, sodium, potassium and chloride (mS · cm^{-2}). (*e*) Chloride fluxes (nmol · cm^{-2} · s^{-1}): apical and basolateral cotransporters and basolateral Goldman. (*f*) Potassium fluxes (nmol · cm^{-2} · s^{-1}): apical cotransport and Goldman and basolateral cotransport and pump. Parameters, $n = 150$.

difference in the lumen between the entrance and the exit of the tubule (Table 2).

This condition could lead to an additional electrodiffusible term (Weinstein, 1994) in the calculation of the total ion quantities in the lumen ($[X]_{lu}$). In contrast with the results reported for the distal tubule (Chang & Fujita, 1999), inclusion of these terms in our cTAL model showed no significant differences in the profiles of the variables presented in Figure 2 (<2.5%). Therefore, the overall salt transport across the tubule wall in the presence and absence of these terms differed by <0.5%, so they were neglected. Furthermore, it has been reported that 20% of total Ca^{2+} is reabsorbed in the ascending limb of Henle's loop (Suki, 1979), and a transepithelial Ca^{2+} permeability of 7.7×10^{-6} cm · s^{-1} was estimated (Bourdeau & Burg, 1979). Simulations have been run with our model using this Ca^{2+} permeability value for the shunt pathway and Ca^{2+} concentrations of 1.2 mM for the fluid at the entrance of the tubule as well as for the extracellular interstitial fluid. The results obtained with and without taking Ca^{2+} fluxes into account differ by <4% for the V_{OC} values calculated. Therefore, Ca^{2+} fluxes were disregarded.

Fitting Experimental Data

Figure 3a shows the dependence of $[Na]_{collected}$ (i.e. $[Na^+]_{lu(n)}$) at the exit of the tubule on the maximum pump flux ($J_{bl(pump,mx)}$). Volume flow rates per unit length (f/L, nl·min^{-1} mm^{-1}) of 0.33, 0.2 and 0.01 have been used in these simulations. The top curves were computed using the reference shunt permeabilities (Table 1; $P_{sh(Na)} = 246 \times 10^{-7}$, $P_{sh(Cl)} = 98 \times 10^{-7}$ and $P_{sh(K)} = 295 \times 10^{-7}$ cm·s^{-1}), while the bottom curves simulate a tighter tubule where the shunt permeabilities for the three ions were reduced to a fraction of their reference values ($P_{sh(X)} = 0.25\ P_{sh(X\_Ref)}$, i.e., $P_{sh(Na)} = 62 \times 10^{-7}$, $P_{sh(Cl)} = 25 \times 10^{-7}$ and $P_{sh(K)} = 74 \times 10^{-7}$ cm s^{-1}). It can be observed that the limiting value for concentration of Na^+ collected at the exit, the Na^+ static head concentration (Burg, 1982), depends only on the shunt conductance. Static heads of 52 and 25 mM were

Table 2. Electrical potential differences across both epithelial barriers and equilibrium potentials for K^+ and Cl^-

	V_{OC}	V_{ap}	V_{bl}	$Eq_{ap}K$	$Eq_{bl}K$	$Eq_{bl}Cl$
entrance	8.03	79.41	−71.39	90.30	−90.30	−45.69
exit	14.09	90.04	−75.95	101.15	−91.27	−52.81
difference	6.06	10.63	−4.56	10.85	−0.97	−7.12

Values of the electrical potential differences and of the K^+ equilibrium potentials across both membrane barriers and the Cl^- equilibrium potential across the basolateral barrier (in m*V*) calculated for the entrance and exit of the tubule in the control state. The last row in the table shows the differences of these variables calculated from the exit to the entrance of the tubule.

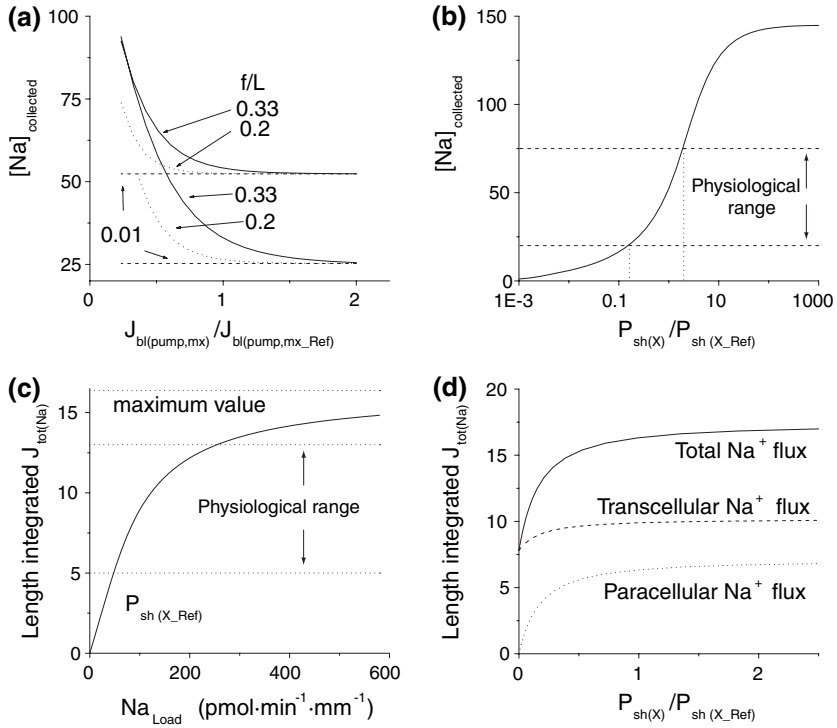

Fig. 3. (*a*) Dependence of concentrations of Na^+ (mM) collected at the tubule exit on the maximum pump flux for three different values of f/L (0.33 for *solid curves*, 0.2 for *dotted curves* and 0.01 nl·min^{-1}·mm^{-1} for *horizontal dashed lines*). *Top curves* simulated using $P_{sh(X\_Ref)}$, while *bottom curves* used $P_{sh(X)} = 0.25\ P_{sh(X\_Ref)}$. (*b*) Static head as a function of $P_{sh(X)}/P_{sh(X\_Ref)}$. A value of f/L equal to 0.01 nl·min^{-1}·mm^{-1} was used in the simulations. *Horizontal lines* show the physiological range. (*c*) Total Na^+ reabsorption (pmol · cm^{-1} · s^{-1}) as a function of Na^+ tubular load (pmol·min^{-1}·mm^{-1}), $[Na]_{lu,i=0} = 145$ mM constant and f/L varying from 0.01 to 4 nl·min^{-1}·mm^{-1}. *Upper horizontal line* is the maximum J_{Na} the model gives at P_{sh_Ref}, the *two lower horizontal lines* show the physiological range. (*d*) Total, transcellular and paracellular Na^+ reabsorption (pmol · cm^{-1} · s^{-1}) as a function of $P_{sh(X)}/P_{sh(X\_Ref)}$. Parameters, $n = 10$.

found using shunt permeabilities of $P_{sh(X\_Ref)}$ (Table 1) and 0.25 $P_{sh(X\_Ref)}$, respectively. The tighter the epithelium for the same maximum pump flux, the lower will be the static head obtained.

The maximum pump flux ($J_{bl(pump,mx)}$) required to reach the static head decreases with the flow rate per tubule length (f/L). A very low f/L (0.01 nl · min^{-1} · mm^{-1}) was used to guarantee that the results reported in Figure 3b correspond to the limiting values for the Na^+ collected (static head). Figure 3b shows the dependence of the static head on the shunt permeabilities. It can be observed that for very leaky epithelia the cTAL has no dilution power while for very tight epithelia the tube is able to remove almost all the Na^+ from the lumen. Published data for values obtained at the exit of cTAL or the beginning of the distal tubule range from 75 mM to as low as 20 mM (Burg, 1982; Gottschalk & Mylle, 1959; Jamison & Gehrig, 1992; Stephenson, 1987). These values were taken as the physiological range and are well within our simulated results.

It has been reported by several authors (Jamison & Gehrig, 1992) that in perfused tubules the overall Na^+ reabsorption increases with the Na^+ tubular load. Figure 3c reports calculations that reproduce these observations. The total Na^+ reabsorption was calculated as the Na^+ flux integrated over the total length of the tubule (length integrated $J_{tot\ (Na)}$, pmol cm^{-2} · s^{-1}) and the tubular load (Na_{Load}, pmol · min^{-1} · mm^{-1}) was calculated as the product (f/L) $[NaCl]_{entrance}$. The horizontal dotted lines are the boundaries of the published experimental values (Burg, 1982; Burg & Green, 1973; Jamison & Gehrig, 1992; Jamison, 1987; Katz et al., 1979) and are well within the calculated values. Figure 3d shows the transcellular and paracellular contributions for the total Na^+ flux as a function of the shunt permeabilities ($P_{sh(X)}$). As expected, the transcellular contribution is roughly constant, while the paracellular contribution has a steeper variation for $P_{sh(X)}/P_{sh(X\_Ref)} < 1$, leading to the increase in the total Na^+ reabsorption observed. These curves were obtained

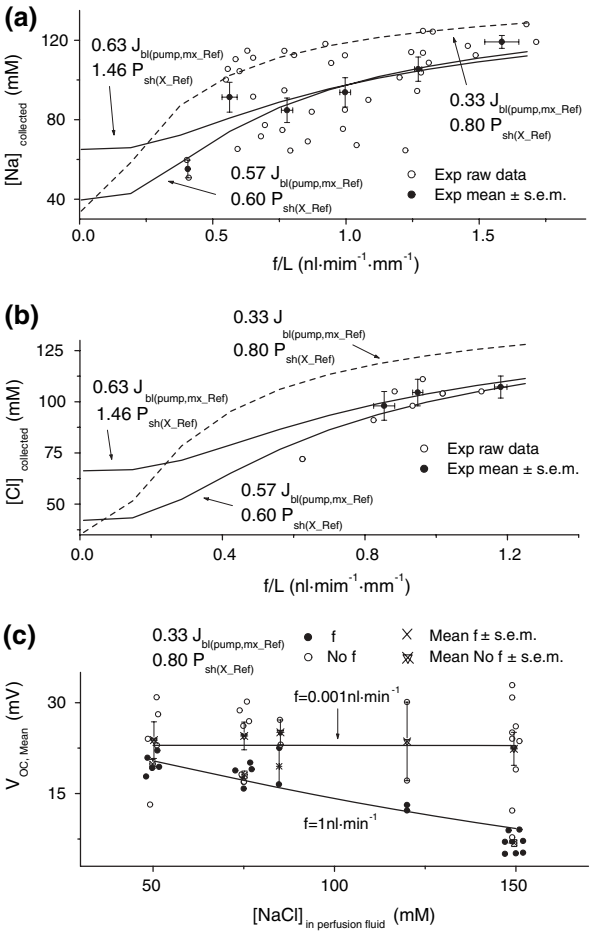

Fig. 4. Experimental data points (raw data and mean ± SEM) adapted from Burg & Green (1973) (concentration values in mM, potential differences in mV and f/L in nl·min^{-1}·mm^{-1}). (*a*) $[Na^+]_{collected}$ as a function of f/L. (*b*) $[Cl^-]_{collected}$ as a function of f/L. (*c*) Mean value of V_{OC} as a function of [NaCl] in the initial perfusate, where the simulated curves were obtained with two different flow rates 1 and 0.001 nl·min^{-1}. *Solid curve* fits in the first two panels (*a, b*) were obtained with the cTAL model using two different sets of parameter values (0.63 $J_{bl(pump,mx\_Ref)}$, 1.46 $P_{sh(X\_Ref)}$ and 0.57 $J_{bl(pump,mx\_Ref)}$, 0.60 $P_{sh(X\_Ref)}$). *Dashed line* in *a* and *b* and the *two solid lines* in *c* were obtained using the same fitting parameters, 0.33 $J_{bl(pump,mx\_Ref)}$ and 0.8 $P_{sh(X\_Ref)}$. Parameters, $n = 10$.

considering high f values so that the tubular load was maximized and the transport capacity was saturated.

For fitting purposes, when a reasonably large number of experimental points was available, they were partitioned into frequency classes and the means and standard errors of the mean (SEM) for each class were computed. The original points and the means ± SEM were plotted together. The best fits to the experimental points were obtained by adjusting the values of the maximum pump flux and the shunt permeabilities ($J_{bl(pump,mx)}$, $P_{sh(X)}$).

Figure 4a and b shows the adapted data taken from Burg & Green (1973) for the Na^+ and Cl^- concentrations in the collected fluid (mM) as a function of f/L (nl · min^{-1} · mm^{-1}). The solid lines show the fits obtained for each variable with two sets of parameters ($J_{bl(pump(mx)} = 0.63$ $J_{bl(pump(mx\_Ref)}$, $P_{sh(X)} = 1.46$ $P_{sh(X\_Ref)}$ and $J_{bl(pump,mx)} = 0.57$ $J_{bl(pump,mx\_Ref)}$, $P_{sh(X)} = 0.60$ $P_{sh(X\_Ref)}$). The dashed lines show the results with the parameters used in the fitting of the V_{OC} (Fig. 4c). Since the experimental conditions and the variables fitted were so different, there was a need to change the fitting parameters without falling into an incoherent choice of parameters between both fittings.

Figure 4c is a plot of the data also taken from Burg & Green (1973) for the V_{OC} (mV) measured as a function of the NaCl concentration (mM) in the perfusion solution with two different flow rate conditions. All data points were corrected for the liquid junction potential that exists in these experiments between the perfusion solution and the bath, using a modified Henderson equation as suggested by Burg & Green. The two experimental conditions ($f = 0.001$ and 1 nl · min^{-1}) were simulated using the same set of

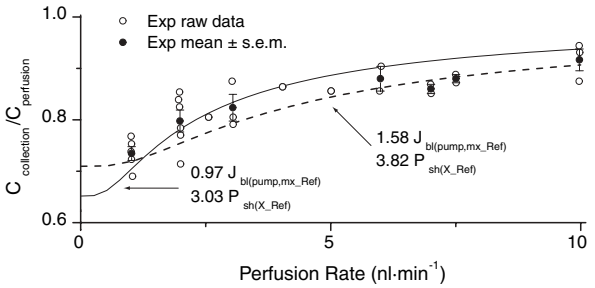

Fig. 5. Dependence of the ratio of osmolarities (collected/perfusion) on perfusion rate. Experimental data points (raw data and mean ± SEM) were adapted from Rocha & Kokko (1973), and curves were obtained with the cTAL model using two sets of parameter values (1.58 $J_{bl(pump,mx\_Ref)}$, 3.82 $P_{sh(X\_Ref)}$ and 0.97 $J_{bl(pump,mx\_Ref)}$, 3.03 $P_{sh(X\_Ref)}$). Parameters, $n = 10$.

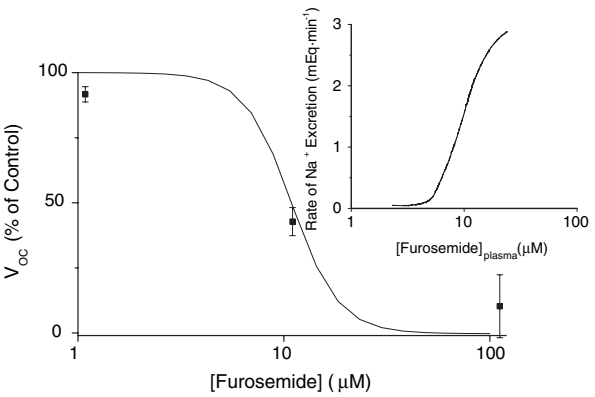

Fig. 6. Experimental data points (raw data and mean ± SEM) adapted from Imai (1977). Dependence of V_{OC} (% control) as a function of furosemide concentration (μM). (*Inset*) Sodium excretion as a function of furosemide plasma concentration, adapted from Brater (1983). Parameters, $n = 10$.

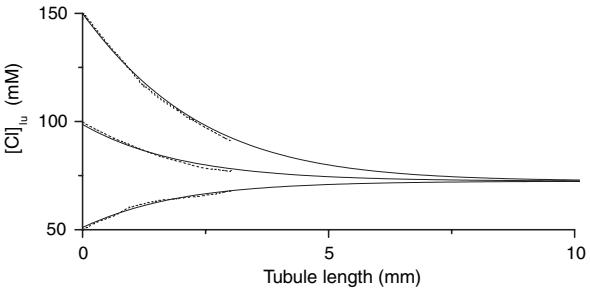

Fig. 7. Simulated curves of the $[Cl]_{lu}$ (mM) as a function of tubule length (mm), adapted from Reeves et al. (1988) (*dashed lines*) and obtained with our model using the same value of $f = 2.5$ nl·min^{-1} (*solid lines*). Values of the adjusted parameters were $J_{bl(pump,mx)} = 0.8\ J_{bl(pump,mx\_Ref)}$ and $P_{sh(X)} = 1.63\ P_{sh(X\_Ref)}$. Parameters, $n = 150$.

parameter values ($J_{bl(pump,mx)} = 0.33\ J_{bl(pump,mx\_Ref)}$, $P_{sh(X)} = 0.80\ P_{sh(X\_Ref)}$ and $K_{ap(cot,Cl)}$ reduced to 15 mM), differing only on the flow rate. A very low value (0.001 nl · min^{-1}) was used to simulate the no-flow experimental condition, while the control value (1 nl · min^{-1}) was used in the flow condition.

Figure 5 reports the dependence of the ratio of the osmolarities (collected/perfusion) on the perfusion rate (f). Rocha & Kokko (1973) obtained the data in outer TAL medullary segments bathed and perfused with ultrafiltrated serum of the same rabbit. The two lines show the fits obtained with the model using two sets of parameter values ($J_{bl(pump,mx)} = 0.97\ J_{bl(pump,mx)}$, $P_{sh(X)} = 3.03\ P_{sh(X\_Ref)}$ and $J_{bl(pump,mx)} = 1.58\ J_{bl(pump,mx\_Ref)}$, $P_{sh(X)} = 3.82\ P_{sh(X\_Ref)}$). These parameters values are in accordance with the fact that the medullar TAL reabsorbs a higher quantity of NaCl but is unable to achieve the dilution observed for the cortical TAL (Jamison & Gehrig, 1992).

In Jamison (1987), the medullary TAL is described as an epithelia leakier and with greater NaCl transport capacity than the cTAL. These characteristics correspond to the higher $P_{sh(X)}$ and $J_{bl(pump,mx)}$ values used in our simulations (Fig. 5).

Figure 6 shows the data points of the dependence of V_{OC} (% control) as a function of furosemide concentration (μM) taken from Imai (1977). The sigmoidal curve represents the simulated dose response of V_{OC} as a function of furosemide concentration obtained with our model. In order to simulate the inhibitory effect of furosemide on the apical cotransporter, we used the reported experimental curve for sodium excretion as a function of furosemidés plasma concentration (Brater, 1983), and from these independent data, the inhibitory kinetic parameters were estimated ($K_{0.5} = 9.8$ μM). According to this inhibitory curve, at the lower concentration tested, 1 μM, no inhibition is found, whereas at 100 μM the cotransport is fully inhibited. We can observe that the behavior of our model follows the pattern of the experimental data points. This is a typical example of the capability of the model to predict the behavior upon given perturbations, based on the selection of a specific parameter value. The model can be used quantitatively as a tool to select the best experimental strategies, by identifying the most sensitive variables to a given parameter perturbation.

Figure 7 displays the simulations published by Reeves et al. (1988) and produced by our model of the Cl^- concentration at the end of the tubule as a function of tubule length (L), when the perfusion fluid had initial concentrations of Cl^- of 150, 100 and 50 mM. The results of Reeves et al. (1988) that coincided with ours were computed for 3-mm tubules with a flow rate 2.5 nl · min^{-1}. As discussed before, we can either increase L or decrease f to obtain the same static head. To have a direct comparison between the results from Reeves et al. (1988) and ours, we chose to keep the same f values and to extend the value of L to an unreal length of 10 mm; the same static head would be obtained by decreasing f values. All curves converged to the same static head at a value of 72.5 mM.

Discussion

The present tubular model brought relevant insight into cTAL performance. Whereas the FF model was limited to simulating data on the cTAL gathered under highly unphysiological conditions (very high perfusion rates, unphysiological baths, etc.), the new tubular version predicts the behavior of cTAL under physiological conditions (micropuncture studies *in situ*) and provides a comprehensive description of the cTAL. The tubular model enables us to calculate the values of the ion concentrations and electrical potential differences at the output of the tubule once they are known at the entry and simulates their steady-state profiles along the tubule. To our knowledge, this latter information has not been obtained experimentally.

Overall the behavior of the TAL is the result of the balance between three quantities: tubular load, tubular reabsorption and tubular leak. The model results show that the first two dominate the performance in the first half of the tubule while the leak grows in importance with the dilution of the tubular fluid and determines the maximum dilution capacity; an extreme example of this effect is the case of Na^+ flux through the junction pathway which changes direction as it approaches the end of the tube.

Simulations of *in vitro* experiments in which the TAL was perfused under a variety of situations show that our model can reproduce the experimental data at low perfusion rates, when the tubular geometry plays an important role. Our model pre-

dicts that the lumenal electrical potential increases from the beginning to the end of the tubule (Table 2). Two components determine this electrical potential profile along the tubule: the transepithelial electrical potential difference and the chemical gradients along the lumen, both reflecting transepithelial salt transport. When TAL is perfused at high rates with a diluted NaCl solution in relation to the bath, the transepithelial electrical potential difference increases from 6.7 to 23.0 mV (Burg et al., 1973). Under similar conditions, the potential difference across the basolateral barrier changes very little (Bell, Lapointe & Cardinal, 1989). Our model simulates both results. The production of an electrical potential gradient along the lumen simulated with our model can be seen as a simple extension of these results.

According to the experimental results of Burg & Green (1973), when tubules were perfused with concentrations of 80 mM of Na^+ the $[Na^+]_{collected}$ decreased, whereas with perfusate concentrations around 50 mM the $[Na^+]_{collected}$ increased. Jamison & Gehrig (1992) also reported that below certain lumen NaCl concentrations the reabsorption process is balanced by an equivalent back-leak. Given a set of parameter values, our model predicts that the same static head is obtained independently of the NaCl concentration at the entrance of the tubule. In Figure 7, the flow rate per unit length considered was the same used by Reeves et al. (1988), where the static head was only obtained at 10 mm, an unreal tubule length. The same static head could be obtained within a 1-mm tubule by increasing the maximum pump flux by a factor of 4 or decreasing the flow rate per unit length to 0.35 nl $\cdot$ min^{-1} $\cdot$ mm^{-1}.

The lowest values reported in the literature for *in vivo* experiments go as low as 20–30 mM NaCl concentration at the end of the tubule (Jamison & Gehrig, 1992). Our model predicts that such a low value can only be obtained for very tight epithelium ($P_{sh(X)} = 0.2\ P_{sh(X\_Ref)}$), where the back-leak is substantially reduced and with a very low flow rate (Fig. 3b).

Throughout, we demonstrated a systematic good agreement between the predicted model results and the experimental data gathered at the entrance and the exit of the cTAL published by independent research groups. Therefore, we are confidant that the present model predicts well the concentration and potential profiles existing along the tubule, to be confirmed if and when experimental observations *in vivo* are feasible.

A greater level of visualization and understanding of the key features of ion transport along the tubule is obtained by use of this model, allowing the design of future experiments. We believe that this model can be particularly useful as a tool to identify the more sensible measurable variables, when perturbations are introduced with drug inhibitors of transporters.

The authors acknowledge Fundação para a Ciência e Tecnologia-Ministério da Ciência e Tecnologia (FCT-MCT) for financial support. F. C. F. also acknowledges financial support from FCT-MCT (SFRH/BPD/19369/2004). The model was developed using the Berkeley Madonna software, generously provided by Robert Macey.

Appendix 1: Glossary

General Symbols

J flux
I current
P permeability
X diffusible ion
Z valence
V electrical potential difference
E dimensionless electrical potential difference
osm osmolarity
volu volume
Q quantity
K affinity constant
G conductance

Subscripts

A nondiffusible species
ap apical cell membrane
bl basolateral cell membrane
c cell compartment
cot cotransport
CP1, *CP2* compartments separated by a barrier
exc extracellular interstitial fluid
i exit of the i^{th} segment of the tubule
lu lumen
M barrier of epithelium
mx maximum transport rate
pump pump
Ref reference state
sh shunt barrier
tot total
Tr specific transporter
X diffusible ion

Nomenclature

$Ab_{(X,i)}$ quantity of ion X absorbed through the apical membrane in the ith segment per unit time, mol s^{-1}
Ar area of the apical membrane for one segment, cm^2, defined as $2\pi r^2 \Delta x$
C_M capacitance of barrier M, 1 $\mu F \cdot cm^{-2}$
$Eq_{M(X,i)}$ equilibrium potential of ion (X) across bar-

rier (M) calculated as $\ln([X]_{CP1}/[X]_{CP2})\ RT/(z_x \cdot F)$, $m\,V$
E_{M_Ref} dimensionless quantity defined as $F \cdot V_{\mathrm{M\_Ref}}/(R \cdot T)$ in the reference state (m V)
E_{OC_Ref} dimensionless quantity defined as $E_{ap\_Ref} + E_{bl\_Ref}$
$E_{M(i)}$ dimensionless quantity defined as $FV_{M(i)}/(R{\cdot}T)$ in the i^{th} segment (mV)
$E_{OC(i)}$ dimensionless quantity defined as $E_{ap(i)} + E_{bl(i)}$
F Faraday's constant, 96,500 C·mol^{-1}
f longitudinal flow through the tubule, nl · min^{-1}
factor dimensionless quantity defined as $F^2/(C_{\mathrm{M}}\,R{\cdot}T)$
$G_{M(X,i)}$ conductance of the barrier (M) for the ion (X), in Fig. 2d, mS · cm^{-2}, and in the text, S · cm^{-2}
I_{tot} total transepithelial current density, μA · cm^{-2}
$J_{M(G,X,i)}$ Goldman flux for the X ion at the M (*ap, bl* or *sh*) barrier in the i^{th} segment, mol · cm^{-2}·s^{-1}
$J_{Tot(X,i)}$ total flux of ion X across epithelium, $J_{Tot(X,i)} = J_{ap(Tot,X,i)} + J_{sh(X,i)}$, mol cm^{-2}·s^{-1}
$J_{M(Tot,X,i)}$ total flux of ion X across M barrier, mol cm^{-2}·s^{-1}
$J_{M(Tr,mx)}$ maximum transport rate for specific transport system Tr (*cot* or *pump*) in the M (*ap* or *bl*) barrier, mol cm^{-2}·s^{-1}
$J_{M(Tr,X,i)}$ mediated flux of specific transport system Tr (*cot* or *pump*) transport system for the X ion at the M (*ap, bl* or *sh*) barrier in the i^{th} segment, mol cm^{-2}·s^{-1}
$K_{M(Tr,X)}$ affinity constant in the M (*ap* or *bl*) barrier of the specific transport system Tr (*cot* or *pump*) for ion X (mM), mmol · dm^{-3}
L tubule length, 1 mm
osm_{CP_Ref} osmolarity of the CP (*c, lu* or *exc*) compartment in the reference state, mOsm
$osm_{CP(i)}$ osmolarity of the CP (*lu* or *c*) compartment in the i^{th} segment, mOsm
$P_{M(X)}$ permeability of the M barrier to the ion X, cm · s^{-1}
Q_{ch} total electrical charge, C
$Q_{c(X,i)}$ quantity of X (Na, K, Cl and A) at the i^{th} segment in the cellular compartment per area of apical membrane, mol · cm^{-2}
$Q_{lu(X,i)}$ quantity of X (Na, K, Cl) at the i^{th} segment in the lumenal compartment, mol
R molar gas constant 8.314 $J \cdot \mathrm{mol}^{-1} \cdot \mathrm{K}^{-1}$
r internal tubule radius, 10 μm
r_{MX} flux ratios M barrier for X ion or transport system used in the reference state (r_{apNa}, r_{apK}, r_{apCl}, r_{blNa}, r_{blcot})
$Sat_{M(Tr\_Ref)}$ dimensionless saturation fraction in the M (*ap* or *bl*) barrier of the transport system Tr (*cot* or *pump*) in the reference state
$Sat_{M(Tr,i)}$ dimensionless saturation fraction in the M (*ap* or *bl*) barrier of the transport system Tr (*cot* or *pump*) in the i^{th} segment
T absolute temperature, 310 K
V_{M_Ref} electrical potential difference across the barrier (M) in the reference state (mV)
$V_{M(i)}$ electrical potential difference across the barrier (M) in the i^{th} segment (mV)
$volu_{c\_Ref}$ cell volume associated with each segment for the reference state, cm^3·cm^{-2}, of apical membrane, defined as $(\pi \cdot (r+\tau)^2 - \pi \cdot r^2) \cdot \Delta x/Ar$
$volu_{c(i)}$ intracellular volume of each segment per area of apical membrane, cm^3·cm^{-2}
$volu_{lu(i)}$ volume of each lumen segment, cm^3; defined as $\pi \cdot r^2 \cdot \Delta x$
$[X]_{CP\_Ref}$ concentration of the X ion in compartment CP (*c, lu* or *exc*) in the reference state, mM
$[X]_{CP(i)}$ concentration of X (Na, K, Cl or A) in compartment CP (*c, lu* or *exc*) in the i^{th} segment, mM
Δx length of each segment, cm
τ tubule wall thicknessm, 1.5 μm

Appendix 2: The Flat Sheet FF Model—Reference State

The strategy used to compute the reference state was adapted from Fernandes & Ferreira (1991) and is presented here for convenience. The reference state is the first part of the flat sheet FF model, where the epithelial cell wall is fully characterized by the values of the specific system parameters ($P_{M(X)}$, $J_{M(Tr,mx)}$, $K_{M(Tr,X)}$). It takes advantage of some values taken directly from the literature and uses these as input variables for the calculation of the remaining parameters. Sets of predefined ratios between ion fluxes and shunt permeabilities and conservation relationships (electroneutrality, isotonicity and mass conservation) are used for these calculations. The Goldman Hodgkin and Katz equation calculates diffusion ion fluxes, while the cotransporters and pump fluxes make use of different kinetics. We review here the set of equations used in the reference state (eq. 1a–32a). All the parameters and variables used in these equations can be found in Appendix 1. The predefined ratios between diffusional and cotransport fluxes across the apical barrier (eq. 1a–3a) establish that the permeability values for Na^+ and Cl^- are very low and the permeability for K^+ is very high (K^+ recirculates across this barrier by entering via the cotransport and leaving through the channels).

$$r_{apNa} = J_{ap(G,Na\_Ref)}/J_{ap(cot\_Ref)} = 0.01 \quad \text{eq.}1a-3a$$

$$r_{apCl} = -J_{ap(G,Cl\_Ref)}/\left(2 \cdot J_{ap(cot\_Ref)}\right) = 0.01$$

$$r_{ap_K} = -J_{ap(G,K\_Ref)}/J_{ap(cot\_Ref)} = 0.99$$

For the basolateral membrane, the predefined ratios establish that the cotransport is responsible for only 30% of total Cl^- flux across this barrier, leaving 70% for the diffusion flux (Greger & Schlatter, 1983), while for Na^+, 99% of the total flux through this barrier is due to the operation of the pump, leaving for the diffusional flux a minimal contribution (eq. 4a–6a).

$$r_{bl\,\mathrm{cot}} = J_{bl(\mathrm{cot},Cl\_\mathrm{Ref})} \Big/ \left(J_{ap(\mathrm{cot},Cl\_\mathrm{Ref})} + J_{ap(G,Cl\_\mathrm{Ref})}\right) = 0.3$$

$$r_{blCl} = J_{bl(G,Cl\_\mathrm{Ref})} \Big/ \left(J_{ap(\mathrm{cot},Cl\_\mathrm{Ref})} + J_{ap(G,Cl\_\mathrm{Ref})}\right) = 0.7$$

$$r_{blNa} = -J_{bl(G,Na\_\mathrm{Ref})} \Big/ J_{bl(pump,Na\_\mathrm{Ref})} = 0.01 \qquad \text{eq.}4a-6a$$

For the shunt pathway, the predefined ratios considered between the shunt permeabilities are as follows:

$$r_{shNa} = P_{sh(Na)} \Big/ P_{sh(Cl)} = 2.5 \qquad \text{eq.}7a-8a$$

$$r_{shK} = P_{sh(K)} \Big/ P_{sh(Cl)} = 3.0$$

Furthermore, electroneutrality is also implicit in the application of Kirchhoff's laws to the flat sheet FF model. Thus, the total current across the apical membrane (I_{ap}) equals the current across the basolateral membrane (I_{bl}) and the total transepithelial current (I_{total}) is the sum of the current that crosses the cellular and the junction (I_{sh}) pathways (eq. 9a–10a).

$$I_{ap} = I_{bl} \qquad \text{eq.}9a-10a$$

$$I_{total} = I_{ap} + I_{sh}$$

The values of these currents are evaluated from the sum of the ionic currents (for Na^+, K^+ and Cl^-) across each barrier (diffusional and transporter, $I_X = z_X\, F\, J_X$, where z_X is the valence of the ion $X = Na^+$, K^+ and Cl^-). As the apical and basolateral cotransporters are both electroneutral, the calculation of these currents reduces to the sum of the diffusional currents in the apical barrier and shunt pathway, while in the case of the basolateral membrane, the contribution of the pump fluxes must be also considered.

$$I_{ap} = F \sum_X z_X J_{ap(G,X\_\mathrm{Ref})} \qquad \text{eq.}11a-13a$$

$$I_{bl} = F\left[\sum_X \left(z_X J_{bl\,(G,X\_\mathrm{Ref})}\right) + J_{bl(pump,Na\_\mathrm{Ref})} + J_{bl(pump,K\_\mathrm{Ref})}\right]$$

$$I_{sh} = F \sum_X z_X J_{sh(G,X\_\mathrm{Ref})}$$

The conservation relationships consider the cells in osmotic equilibrium with the extracellular interstitial fluid, and electroneutrality is assumed in all compartments. Eqs. 14a–15a encode these relations for the cellular compartment, where osm_{exc} is the osmolarity of the extracellular interstitial fluid. These equations are used to calculate z_A and $[A]_{c\_\mathrm{Ref}}$:

$$[Na]_{c\_\mathrm{Ref}} + [K]_{c\_\mathrm{Ref}} + [Cl]_{c\_\mathrm{Ref}} + [A]_{c\_\mathrm{Ref}} = osm_{exc}$$

$$[Na]_{c\_\mathrm{Ref}} + [K]_{c\_\mathrm{Ref}} - [Cl]_{c\_\mathrm{Ref}} + z_A [A]_{c\_\mathrm{Ref}} = 0 \qquad \text{eq.}14a-15a$$

Given the values of $volu_{c\_\mathrm{Ref}}$ (Appendix 1) and of $[A]_{c\_\mathrm{Ref}}$, the total quantity of nondiffusible species is as follows:

$$Q_A = [A]_{c\_\mathrm{Ref}} \cdot volu_{c\_\mathrm{Ref}} \qquad \text{eq.}16a$$

The Goldman Hodgkin and Katz equation for the diffusional ion fluxes is as follows:

$$J_{M(G,X\_\mathrm{Ref})} = P_{M(X)} \qquad \text{eq.}17a-25a$$

$$\cdot \left([X]_{CP1\_\mathrm{Ref}} \cdot e^{z_X \cdot E_{M\_\mathrm{Ref}}} - [X]_{CP2\_\mathrm{Ref}}\right) z_X$$

$$\cdot E_{M\_\mathrm{Ref}} \Big/ \left(e^{z_X \cdot E_{M\_\mathrm{Ref}}} - 1\right)$$

E_{M_Ref} and E_{OC_Ref} are defined in Appendix 1.The kinetic equations for the different mediated fluxes were taken directly from the flat sheet FF model. For the Na^+-K^+ pump, the fluxes for Na^+ and K^+ were calculated as follows:

$$J_{bl(pump,Na\_\mathrm{Ref})} = J_{bl(pump,mx\_\mathrm{Ref})} \cdot Sat_{bl(pump\_\mathrm{Ref})} \qquad \text{eq.}26a-27a$$

$$J_{bl(pump,K\_\mathrm{Ref})} = -(2/3) \cdot J_{bl(pump,Na\_\mathrm{Ref})}$$

with

$$Sat_{bl(pump\_\mathrm{Ref})} = \left[1 \Big/ \left[1 + \frac{K_{bl(pump,Na)}}{[Na]_{c\_\mathrm{Ref}}}\right]\right]^3 \cdot \left[1 \Big/ \left[1 + \frac{K_{bl(pump,K)}}{[K]_{exc\_\mathrm{Ref}}}\right]\right]^2$$

For the Na^+-K^+-$2Cl^-$ cotransport, the fluxes for the three ions were calculated as follows:

$$J_{ap(\mathrm{cot},Na\_\mathrm{Ref})} = J_{ap(\mathrm{cot},mx\_\mathrm{Ref})} \cdot Sat_{ap(\mathrm{cot}\_\mathrm{Ref})} \qquad \text{eq.}28a-30a$$

$$J_{ap(\mathrm{cot},K\_\mathrm{Ref})} = J_{ap(\mathrm{cot},Na\_\mathrm{Ref})}$$

$$J_{ap(\mathrm{cot},Cl\_\mathrm{Ref})} = 2 \cdot J_{ap(\mathrm{cot},Na\_\mathrm{Ref})}$$

with

$$Sat_{ap(\mathrm{cot}\_\mathrm{Ref})} = \left[1 \Big/ \left[1 + \frac{K_{ap(\mathrm{cot},Na)}}{[Na]_{lu\_\mathrm{Ref}}}\right]\right]$$

$$\cdot\left[1\Big/\left[1+\frac{K_{ap(\cot,K)}}{[K]_{lu\_\mathrm{Ref}}}\right]\right]\cdot\left[1\Big/\left[1+\frac{K_{ap(\cot,Cl)}}{[Cl]_{lu\_\mathrm{Ref}}}\right]\right]^2$$

$$-\left[1\Big/\left[1+\frac{K_{ap(\cot,Na)}}{[Na]_{c\_\mathrm{Ref}}}\right]\right]\cdot\left[1\Big/\left[1+\frac{K_{ap(\cot,K)}}{[K]_{c\_\mathrm{Ref}}}\right]\right]$$

$$\cdot\left[1\Big/\left[1+\frac{K_{ap(\cot,Cl)}}{[Cl]_{c\_\mathrm{Ref}}}\right]\right]^2$$

For the K^+-Cl^- cotransport, the fluxes for the two ions in the basolateral membrane were calculated as follows:

$$J_{bl(\cot,K\_\mathrm{Ref})} = J_{bl(\cot,mx\_\mathrm{Ref})} \cdot Sat_{bl(\cot\_\mathrm{Ref})}$$

$$J_{bl(\cot,Cl\_\mathrm{Ref})} = J_{bl(\cot,K\_\mathrm{Ref})}$$

with

$$Sat_{bl(\cot\_\mathrm{Ref})} = [Cl]_{c\_\mathrm{Ref}}[K]_{c\_\mathrm{Ref}} - [Cl]_{exc\_\mathrm{Ref}}[K]_{exc\_\mathrm{Ref}} \qquad \text{eq.}31a-32a$$

Computation Strategy

Given all the predefined relations stated above, in the steady-state and open circuit conditions (Greger, 1985) the cTAL model represented in Figure 1 considers that around two Cl^- ions per Na^+ cross the cells, generating a circulating current (I_{cc}) that flows through the cells from the lumen to the extracellular interstitial and back through the junction pathway (eq. 9a–10a, $I_{total} = 0$, $I_{cc} = I_{ap} = I_{bl} = -I_{sh}$). The values used as input variables in the reference state are I_{cc}, the eight ratios defined in eq. 1a–8a, the potential differences V_{ap} and V_{bl} (consequently E_{ap} and E_{bl}), the nine concentrations of the three ions in all compartments $[X]_{CP\_\mathrm{Ref}}$, the osmolarity osm_{exc}, the five affinity constants of the transporters and the cell volume $volu_{c\_\mathrm{Ref}}$. In spite of assuming a flat sheet geometry and to ensure consistency between reference state and tubular module, $volu_{c\_\mathrm{Ref}}$ is calculated on the basis of the tridimensional structure of the tube: r, τ and $(\Delta x$ (see Appendix 1). The output variables of the reference state are the maximum capacity of the transporters $J_{M(Tr,mx)}$, the nine permeabilities $P_{M(X)}$ and the quantity Q_A and valence of the nondiffusible species z_A. The input and output values are listed in Table 1.

References

Bell, P.D., Lapointe, J.Y., Cardinal, J. 1989. Direct measurement of basolateral membrane potentials from cells of the macula densa. *Am. J. Physiol.* **257:**F463–F468

Bourdeau, J.E., Burg, M.B. 1979. Voltage dependence of calcium transport in the thick ascending limb of Henle's loop. *Am. J. Physiol.* **236:**F357–F364

Brater, D.C. 1983. Pharmacodynamic considerations in the use of diuretics. *Annu. Rev. Pharmacol. Toxicol.* **23:**45–62

Burg, M., Stoner, L., Cardinal, J., Green, N. 1973. Furosemide effect on isolated perfused tubules. *Am. J. Physiol.* **225:**119–124

Burg, M.B. 1982. Thick ascending limb of Henle's loop. *Kidney Int.* **22:**454–464

Burg, M.B., Green, N. 1973. Function of the thick ascending limb of Henle's loop. *Am. J. Physiol.* **224:**659–668

Chang, H., Fujita, T. 1999. A numerical model of the renal distal tubule. *Am. J. Physiol.* **276:**F931–F951

Fernandes, P.L., Ferreira, H.G. 1991. A mathematical model of rabbit cortical thick ascending limb of the Henle's loop. *Biochim. Biophys. Acta* **1064:**111–123

Gottschalk, C.W., Mylle, M. 1959. Micropuncture study of the mammalian urinary concentrating mechanism: Evidence for the countercurrent hypothesis. *Am. J. Physiol.* **196:**927–936

Greger, R. 1981. Cation selectivity of the isolated perfused cortical thick ascending limb of Henle's loop of rabbit kidney. *Pfluegers Arch* **390:**30–37

Greger, R. 1985. Ion transport mechanisms in thick ascending limb of Henle's loop of mammalian nephron. *Physiol. Rev.* **65:**760–797

Greger, R., Oberleithner, H., Schlatter, E., Cassola, A.C., Weidtke, C. 1983. Chloride activity in cells of isolated perfused cortical thick ascending limbs of rabbit kidney. *Pfluegers Arch.* **399:**29–34

Greger, R., Schlatter, E. 1983. Properties of the lumen membrane of the cortical thick ascending limb of Henle's loop of rabbit kidney. *Pfluegers Arch.* **396:**315–324

Greger, R., Weidtke, C., Schlatter, E., Wittner, M., Gebler, B. 1984. Potassium activity in cells of isolated perfused cortical thick ascending limbs of rabbit kidney. *Pfluegers Arch.* **401:**52–57

Imai, M. 1977. Effect of bumetanide and furosemide on the thick ascending limb of Henle's loop of rabbits and rats perfused in vitro. *Eur. J. Pharmaco.* **41:**409–416

Jamison, R.L. 1987. Short and long loop nephrons. *Kidney Int.* **31:**597–605

Jamison, R.L., Gehrig, J.J.J. 1992. Urinary concentration and dilution: Physiology. *In:* Windhager, E., (editors) Handbook of Physiology. Renal Physiology, sect. 8. pp 1219–1279, American Physiological Society/Oxford University Press, New York

Katz, A.I., Doucet, A., Morel, F. 1979. Na-K-ATPase activity along the rabbit, rat, and mouse nephron. *Am. J. Physiol.* **237:**F114–F120

Macey R., Oster G., Zahnley T. 2003. Berkeley Madonna User's Guide, version 8.0 (http://www.berkeleymadonna.com)

Oberleithner, H., Lang, F., Wang, W., Giebisch, G. 1982. Effects of inhibition of chloride transport on intracellular sodium activity in distal amphibian nephron. *Pfluegers Arch.* **394:**55–60

Reeves, W.B., Molony, D.A., Andreoli, T.E. 1988. Diluting power of thick limbs of Henle. III. Modulation of in vitro diluting power. *Am. J. Physiol.* **255:**F1145–F1154

Rocha, A.S., Kokko, J.P. 1973. Sodium chloride and water transport in the medullary thick ascending limb of Henle. Evidence for active chloride transport. *J. Clin. Invest.* **52:**612–623

Stephenson, J. 1992. Urinary concentration and dilution: Models. *In:* Windhager, E.E.., (editors) Handbook of Physiology. Renal Physiology, sect. 8. pp 1349–1408, American Physiological Society/Oxford University Press, New York

Stephenson, J.L. 1987. Models of the urinary concentrating mechanism. *Kidney Int.* **31:**648–661

Suki, W.N. 1979. Calcium transport in the nephron. *Am. J. Physiol.* **237:**F1–F6

Weinstein, A.M. 1994. Mathematical models of tubular transport. *Annu. Rev. Physiol.* **56:**691–709

Weinstein, A.M. 2003. Mathematical models of renal fluid and electrolyte transport: Acknowledging our uncertainty. *Am. J. Physiol.* **284:**F871–F884

Wexler, A.S., Kalaba, R.E., Marsh, D.J. 1991. Three-dimensional anatomy and renal concentrating mechanism I. Modeling results . *Am. J. Physiol.* **260:**F368–F383

Wirz, H., Hargitay, B., Kuhn, W. 1951. Localization of the concentration process in the kidney by direct kryoscopy. *Helv. Physiol. Pharmacol. Acta* **9:**196–207